B2

ORNL-4288
UC-38 – Engineering and Equipment

ATTENUATION OF SHOCK WAVES IN LONG PIPES BY ORIFICE PLATES, ROUGH WALLS, AND CYLINDRICAL OBSTACLES

Lawrence Dresner
Conrad V. Chester

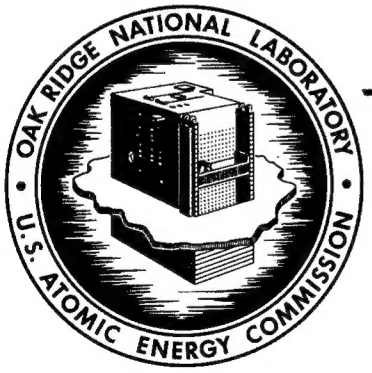

OAK RIDGE NATIONAL LABORATORY
operated by
UNION CARBIDE CORPORATION
for the
U.S. ATOMIC ENERGY COMMISSION

Send by Joe Deal.
for Comments
Answer 2 8/28/68

Printed in the United States of America. Available from Clearinghouse for Federal
Scientific and Technical Information, National Bureau of Standards,
U.S. Department of Commerce, Springfield, Virginia 22151
Price: Printed Copy $3.00; Microfiche $0.65

ORNL-4288

Contract No. W-7405-eng-26

Director's Division

CIVIL DEFENSE RESEARCH PROJECT

ATTENUATION OF SHOCK WAVES IN LONG PIPES BY ORIFICE PLATES, ROUGH WALLS, AND CYLINDRICAL OBSTACLES[1]

Lawrence Dresner and Conrad V. Chester

(1) Research sponsored by the Advanced Research Projects Agency of the Department of Defense pursuant to a letter of agreement with the Atomic Energy Commission under Advanced Research Projects Agency Order No. 907.

JULY 1968

OAK RIDGE NATIONAL LABORATORY
Oak Ridge, Tennessee
operated by
UNION CARBIDE CORPORATION
for the
U.S. ATOMIC ENERGY COMMISSION

CONTENTS

ABSTRACT

This paper reports exploratory measurements of the attenuation of shock waves in tubes by orifice plates, rough walls, and cylindrical obstacles. The measurements were carried out in a four-inch shock tube driven by an explosive mixture of propane and oxygen. It appears possible to correlate the attenuation produced by obstacles placed in the flow with their Fanning friction factors. The orifice plates and cylindrical obstacles are very efficient attenuators.

ATTENUATION OF SHOCK WAVES IN LONG PIPES BY ORIFICE PLATES, ROUGH WALLS, AND CYLINDRICAL OBSTACLES

Lawrence Dresner and Conrad V. Chester

1. INTRODUCTION

Providing blast protection for urban populations is one of the most important problems of civil defense, one which has been under study at the Oak Ridge National Laboratory for the past several years. A requirement set at ORNL for blast shelters is that whatever their nature, they should be interconnected so as to permit movement of people and supplies. It soon became clear that the interconnecting tunnels themselves could serve as shelters, and this led to the concept of an underground grid of interconnected tunnels. E. P. Wigner has described such a tunnel-grid system in detail in the proceedings of a 1965 symposium of the American Association for the Advancement of Science on civil defense.[1]

Access to the tunnels in this system is through air locks, which prevent shock waves from reaching the interior of the tunnel complex. Unfortunately, air locks are expensive. Blast doors, an alternative to air locks, may also be expensive and furthermore do not permit continuous access to the tunnels. We have therefore examined other ways of protecting the interiors of long open tunnels from shock waves. Baffling the tunnel entrances with orifice plates is a way of doing this, and one purpose of this paper is to report experiments exploring its effectiveness.

A second purpose is to report the results of experiments on the attenuation of shock waves by artificially roughened walls and by cylindrical obstacles placed in the path of the shock. In addition to possible practical applications these experiments may have, they serve, together with the experiments on the orifice plates, to support a rough empirical correlation of shock attenuation with the Fanning friction factor that would govern fully developed turbulent flow in the same pipe at the Reynolds number of the flow behind the shock front.

Finally, a third purpose of this paper is to describe the four-inch shock tube in which the experiments were carried out. It is driven by an explosive mixture of propane and oxygen, and exhibits some interesting gas-dynamic effects that are worthy of note.

2. EQUIPMENT

The shock tube is made up of lengths of schedule-40, 4-inch iron pipe (wall thickness: 0.237"); schedule-80, 4-inch Hastelloy pipe (wall thickness: 0.337"); and schedule-XX, 5-inch stainless steel pipe (wall thickness: 0.750"). The different sections of pipe, which vary from 2 to 8 feet in length, are joined with Grayloc (Gray Tool Co.) flanges. Grayloc flanges are much more convenient than screwed connections, minimizing the manipulation involved in changing the pipes around. Each section of pipe rides on its own steel cart, so that the pipes can be moved simply by loosening the Grayloc flanges, wheeling the carts around, and retightening the Grayloc flanges.

A quick-release Grayloc flange clamps the membrane separating the explosive gas mixture from the rest of the shock tube. Only one bolt has to be loosened to free the quick-release flange, after which it rides smoothly out of the way on a counter-weighted cable. Since the membrane has to be changed after every explosion, the quick-release flange is a great convenience.

The membrane is made of polyethylene reinforced by Dacron scrim. A four-inch-diameter span will support a static pressure of more than 100 psi, so the section containing the explosive gas mixture may be pressurized to increase the explosive yield.

Piezoelectric quartz transducers (Kistler 603A, 606L, and 613F) measure pressure as a function of time at various positions down the shock tube. The amplified signals from the transducers are displayed by two oscilloscopes, whose faces are photographed with Polaroid cameras. The transducers, some of which differ from others in size, are all mounted in standardized bushings made from one-inch bolts. One-inch nuts have been welded to the wall of the schedule-40 pipe every four inches and the pipe wall drilled out. The holes are plugged with solid bolts except at the measuring stations, where the transducers are mounted in their bushings. Measuring stations can thus be changed merely by interchanging two bolts.

The explosive mixture used in the experiments reported below consists of 79% oxygen and 21% propane. It results from charging the driver section by flushing it thoroughly with compressed oxygen, bleeding it down to atmospheric pressure through a small valve, and then admitting 20-cm-Hg of propane under pressure. The gauge pressure of the

driver at detonation is then 20 cm-Hg. The gas mixture is detonated by a .22-caliber blank cartridge discharged into it by a rifle mounted in the end cap of the shock tube.

3. RESULTS: BARE TUBE

The shock overpressure in the bare shock tube is the reference by which we judge the attenuation produced by the different kinds of baffles. Fig. 1 shows shock overpressures measured at various distances X down the shock tube; X is measured from the end cap, and is given in units of L, the length of the driver section. These overpressures were measured by timing the flight of the shock between a pair of transducers located four inches apart and then converting the measured shock velocity to overpressure using the Rankine-Hugoniot equations. We consider this method of measuring shock overpressures superior to the use of a single transducer for the following three reasons. First, the transducers are sensitive to acceleration and respond to mechanical vibrations induced by the passage of the shock. These vibrations produce a high-frequency background signal which makes it difficult to determine the shock overpressure. Second, the reading of the transducer seems to vary somewhat with the conditions of service: we have observed that simply removing a transducer from its mounting and replacing it again changes its reading, sometimes by as much as 20%. Third, when compared with overpressures determined from shock velocities, directly measured overpressures appear to be about 25% low on the average.

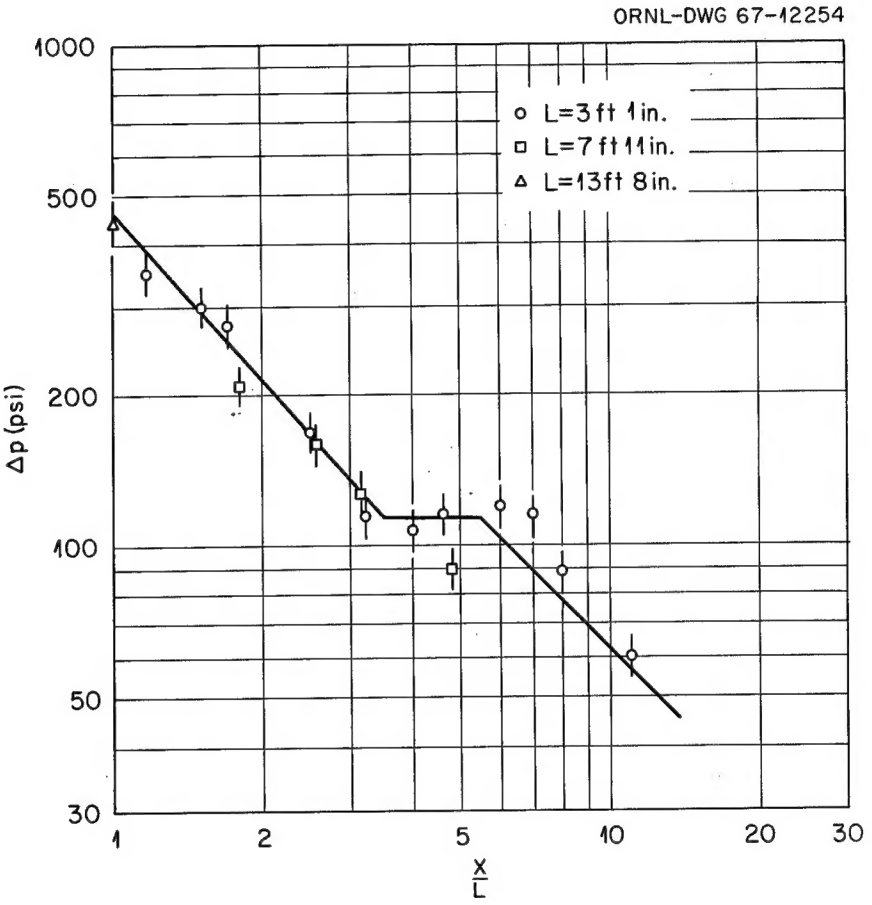

Figure 1. Peak overpressure as a function of distance down the bare shock tube. Δp is the overpressure, X the distance down the tube, and L the length of the driver section. The points are experimental; the curve has been calculated (see discussion below).

The triangular point lying at X = L in Fig. 1 was determined in a slightly different way from the others. When first measured using the Dacron-reinforced polyethylene membrane, the peak overpressure at X = L was about 300 psi, about 30% lower than would be estimated from the points lying between X/L = 1.5 and X/L = 3.5. On the basis of this measurement, the experimental overpressure-distance curve would have a maximum near X = L, contrary to theoretical expectations, as we shall see below. We hypothesized that the reduction in overpressure near X = L is connected with the use of a fairly massive membrane. To test this hypothesis, we performed measurements with much thinner membranes made of Saran Wrap. We backed up the Saran Wrap with a Dacron-reinforced membrane and filled the driver section with the explosive gas mixture in the usual way. Then after the gases were thoroughly mixed, we bled the pressure in the driver section down to one atmosphere, removed the Dacron-reinforced back-up membrane, and fired the shock tube. The overpressure measured in this way at X = L was about 365 psi, but this figure needs to be corrected for the fact that the pressure in the driver section was only 76 cm-Hg instead of 96 cm-Hg. For this small difference in driver pressures, the correction, derived from numerical calculations similar to the one described below, is very close to the ratio of the driver pressures, 96/76 = 1.26. Thus the overpressure that should be plotted at X = L is 365 x 1.26 = 460 psi; this is the value actually shown.

The square point at X/L = 4.8 is a little lower than the circular points in this neighborhood; this appears to be due to frictional losses in the bare pipe and will be discussed further in Sec. 4.

The points shown are averages of several measurements. The variation about the mean is about 10%; the error bars in Fig. 1 have arbitrarily been chosen to correspond to an error of ± 10%.

It is possible to calculate the curve of overpressure versus distance down the shock tube; by comparing calculation and experiment it is possible to determine the total energy of the blast wave created by the explosion.

The overpressure p at any point X down the tube is a function of X, E, L, p_o, and ρ_o, where E is the energy per unit face area of shock front in the blast wave, and p_o and ρ_o are the initial pressure and density in the shock tube. Here we have assumed the initial pressure and density in the driver section are also p_o and ρ_o before the explosion. If $\Delta p \gg p_o$, the dependence of Δp on p_o can be neglected. This assumption is equivalent to saying that the air molecules are at rest rather than in a state of thermal agitation before they are struck. If the velocity of the molecules of the shocked air is much greater than the velocities of thermal agitation, this is a good assumption. A simple dimensional analysis then shows that Δp must depend on the remaining variables as follows:

$$\Delta p = \frac{E}{L} f\left(\frac{X}{L}\right) \qquad (1)$$

where f is as yet an undetermined function. In general, f depends on the nature of the two gases, which enters here through their ratios of specific heats, and on the details of how the energy E is initially

released in the driver section.

The initial data in the calculation of the function f are the pressure, density, and velocity distributions behind the detonation front at the instant it reaches the membrane. The wave diagram corresponding to this initial data is that of a Chapman-Jouguet detonation followed by a rarefaction wave. Because the flow behind a Chapman-Jouguet detonation is sonic relative to the front, the leading edge of the rarefaction coincides with the detonation front. Behind the rarefaction is a region of stationary burned gas of uniform pressure and density. The detailed computation of the initial data is described in reference 2; the results are summarized below:

For $x/L \geq 1/2$,

$$p = 2\rho_o q_o (\gamma-1) \left[\frac{1}{\gamma} + \frac{\gamma-1}{\gamma} \frac{x}{L}\right]^{\frac{2\gamma}{\gamma-1}} \tag{2a}$$

$$\rho = \rho_o \frac{\gamma+1}{\gamma} \left[\frac{1}{\gamma} + \frac{\gamma-1}{\gamma} \frac{x}{L}\right]^{\frac{2}{\gamma-1}} \tag{2b}$$

$$u = \frac{2U}{\gamma+1} \left[\frac{x}{L} - \frac{1}{2}\right] \tag{2c}$$

$$U = \left[2(\gamma^2 - 1)q_o\right]^{\frac{1}{2}} ;$$

for $x/L < 1/2$, $p=p(1/2)$, $\rho=\rho(1/2)$, and $u=u(1/2)=0$. (2d)

Here p, ρ, and u are respectively the pressure, density, and flow velocity at any point x behind the membrane at the instant the detonation front reaches L, the position of the membrane. q_o is the energy released by combustion per gram of reactants. U is the velocity of the

detonation front, and γ is the ratio of the specific heats of the burned gas. Eqs. (2) are based on the assumption that $p \gg p_o$.

The correct value of γ to use in Eqs. (2a-c) can be estimated from Eq. (2d) using the measured detonation velocity U and an estimate of the energy release q_o. According to measurements of Breton quoted by Lewis and von Elbe,[3] the detonation velocity of a 21%-79% propane-oxygen mixture is very close to 2.50 km sec^{-1} at atmospheric pressure and is nearly independent of pressure. For the stoichiometric combustion of propane and oxygen to carbon monoxide and water vapor, q_o = 1.83 kilocal g^{-1}. Using these values in Eq. (2d), we find that γ = 1.19.

Fig. 2 shows two curves of overpressure versus distance calculated by the method of von Neumann and Richtmyer[4] using the initial data given in Eqs. (2). The upper of the two curves is based on the assumption that the γ of the burned gas and that of the air are the same, namely, 1.4. The lower of the two curves is based on the assumption that the γ of the burned gas is 1.2. Comparison of the two curves shows how important it is to use the correct value of γ in estimating E. It is gratifying that the curves reproduce the "plateau" present in the experimental points in the neighborhood of X/L = 3-7; however, the experimental plateau is somewhat wider than the theoretical one. This plateau is caused by the forward expansion of the stationary gas behind the rarefaction wave that follows the detonation front. This expansion catches up with the shock front in the vicinity of X/L = 3 and supports the shock front for about two driver lengths. This can be seen clearly from a time-sequence of pressure, density, and velocity profiles given in reference 2.

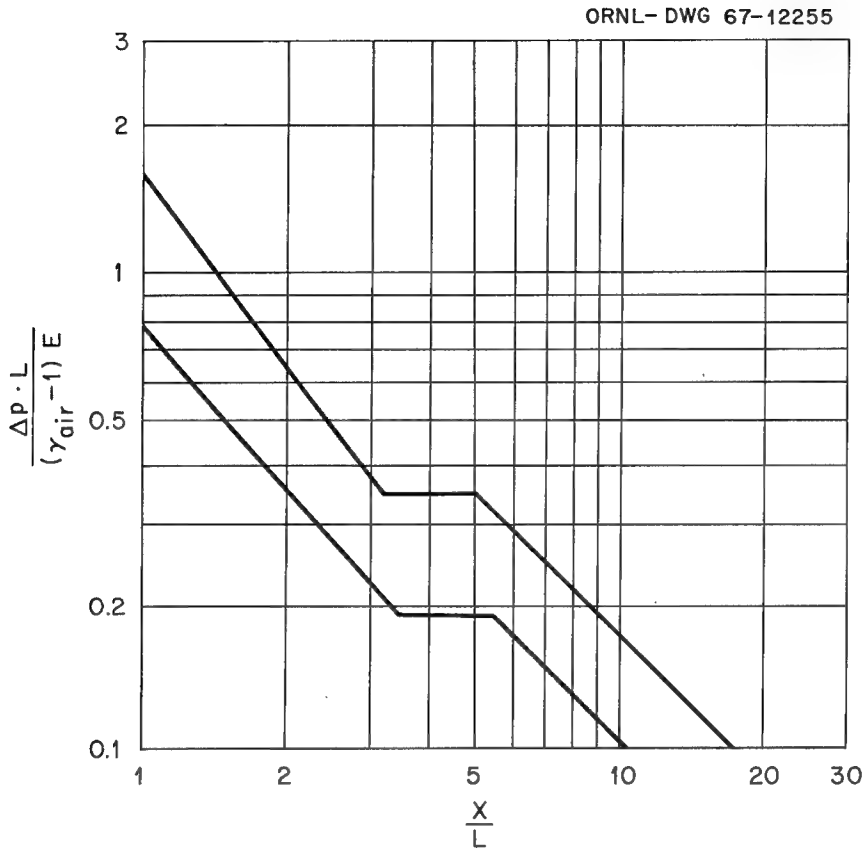

Figure 2. Theoretical peak overpressure as a function of distance down a bare tube. Δp is the overpressure, L the length of the driver section. γ_{air} the ratio of the specific heats of air, E the energy released in the explosion divided by the cross-sectional area of the shock tube, and X the distance down the shock tube. The upper curve is based on the assumption that the combustion products have the same ratio γ of specific heats as air; the lower curve is based on the assumption that $\gamma = 1.2$ for the combustion products and $\gamma = 1.4$ for the shocked air.

Shown in Fig. 1 is the lower of the two curves in Fig. 2, corresponding to a γ for the burned gas of 1.2, normalized to a yield in air blast of 1.26 kilocal per gram of reactants, or about 70% of what would be expected from the combustion of the propane in the driver mixture to carbon monoxide and water vapor. The remaining energy of combustion is lost to the walls as heat. A yield in air blast of 1.26 kilocal g^{-1} corresponds to a yield of 6 g TNT per running foot of driver section in a four-inch shock tube driven with the propane-oxygen mixture described above.

4. RESULTS: BAFFLED TUBES

Four sets of experiments were carried out with orifice plates, the sets differing in either spacing or inner diameter of the orifice plates. In three sets of experiments, the inner diameter of the orifice plates was 3-1/8" and the spacing either 4", 8", or 12". In the fourth experiment, the spacing was 4" and the inner diameter $2\frac{1}{2}$". In the experiments using a four-inch spacing, space for 31 orifice plates was provided, but in fact only 28 were used, numbers 8, 16, and 24 having been removed. This was done so that clear spaces eight inches wide were available in which the transducer pairs could be mounted without having an orifice plate between them. No such omission was necessary with the eight- or twelve-inch spacing. 16 baffles were used with the eight-inch spacing and 12 baffles were used with the twelve-inch spacing. In the experiments carried out with the 3-1/8" orifice

plates, the first orifice plate was always placed 9'8" from the end cap of the shock tube; the length of the driver in these experiments was 37". Two driver lengths were used in the experiments carried out with the $2\frac{1}{2}$" baffles, 37" and 95". With the smaller driver, the first baffle was located at 10'3", with the larger, at 15'2". The shock overpressure was measured at intervals of approximately 2'6".

The overpressures measured in these experiments are plotted in Fig. 3, which is a replica of Fig. 1. Shown also are curves obtained by applying to the curve in Fig. 1 a correction factor C given by

$$C = \exp(-0.30\ f\ \Delta X/D) \qquad (3)$$

where

f is the Fanning friction factor that applies to fully developed turbulent flow in the section of pipe containing the orifice plates at a Reynolds number equal to that of the flow behind the shock front,

ΔX is the distance from the beginning of the baffled section of the point of interest, and

D is the diameter of the pipe.

It is tacitly assumed that the friction factor is constant over the range of Reynolds numbers covered. The Reynolds number of the flow behind a 100-psi shock in a four-inch pipe is about 6×10^6; for a 10-psi shock it is about 1×10^6. In a smooth pipe[5], the friction factors corresponding to these Reynolds numbers differ only about 32%; thus the variation of the Reynolds number about some suitable mean is

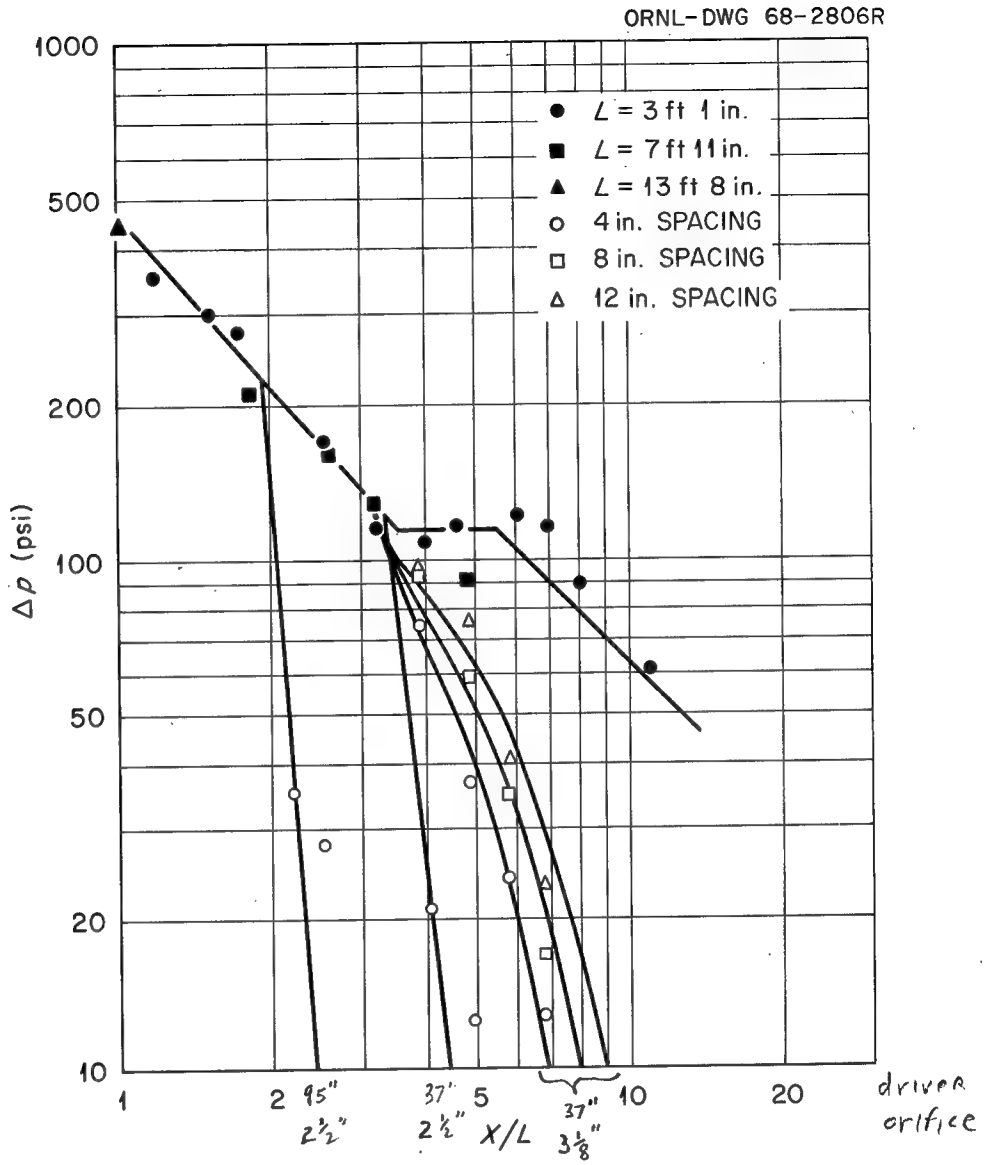

Figure 3. Peak overpressure in a tube containing orifice plates. Δp is the overpressure, X the distance down the tube, and L the length of the driver section. The black points are taken from Fig. 1 and refer to the bare tube. The open points refer to positions inside the baffled section. From left to right, the five lower curves refer, respectively, to 2-1/2" orifice plates with a 7'11" driver, 2-1/2" orifice plates with a 3'1" driver, and 3-1/8" orifice plates with a 3'1" driver (rightmost three curves). The lower curves have been calculated by applying the correction factor of Eq. (3) to the upper curve.

only of the order of 16%. For rough pipes[5], the variation is even less. In fact, for an equivalent sand roughness of more than 10^{-4}, the friction factor is constant above a Reynolds number of 10^6.

Arredi[6] and Möbius[7] have reported measurements of the friction factors for configurations of orifice plates. Their measurements cover the range of inner diameters and spacings used in our experiments mentioned above. By interpolating in their data, we find f = 0.21, 0.15, and 0.12 for the 3-1/8" orifice plates according as their spacing is 4", 8", or 12", and f = 0.78 for the 2.5" orifice plates at a 4" spacing. The data indicate that f is nearly constant above a Reynolds number of 10^4.

Eq. (3) is a satisfactory correlation of the experiments, which cover a range of about a factor of six in friction factor. In order to try to cover a wider range of friction factors, we performed an experiment in which the friction factor was reduced by approximately an order of magnitude below the smallest value it had in the experiments with the orifice plates. The wall of the shock tube was artificially roughened by cutting a V-thread in it with an apex angle of 60° and a pitch of 0.125". Thus the depth-to-pitch ratio is 0.866 and the depth-to-diameter ratio in a four-inch pipe is 0.0271. Schiller[8] has reported values of f for various "Löwenherz" threads (metric threads with a depth-to-pitch ratio of 0.75 and flats at top and bottom equal to one-eighth of the pitch). In one of his experiments, the depth-to-diameter ratio was 0.0286; the corresponding value of f was about 0.013. Schiller's data also indicate that f

becomes constant above a Reynolds number of 10^5.

Shown in Fig. 4 are results of experiments carried out with the threaded wall; the driver length was again 37" and the threaded section began 9'8" from the end cap. Shown also is a curve obtained by applying the correction given by Eq. (3) with f = 0.013 to the curve in Fig. 2. Agreement is not bad, although the curve clearly lies slightly above the mean course of the points. The comparison of the correlation (3) and the data is complicated by the presence of an unexplained fine structure in the experimental points that takes the form of a slight minimum near X/L = 4 and a slight maximum near X/L = 6. If instead of using the curve in Fig. 1 as the reference pressure to which to apply the correction C, we use the actual measured points in the bare tube, the correlation is significantly worsened.

In the last set of experiments, aluminum dowels 1/2" in diameter and 2-1/2" long obstructed the flow. The dowels were screwed rigidly into a base plate containing a triangular array of holes shown in Fig. 5. Five different patterns were used, all of which are also shown in Fig. 5. The full-density pattern contains 8 dowels per diameter of length; of the remaining four patterns, two correspond to two-thirds density, and two to one-third density.

Shown in Figs. 6 a-e are overpressures measured at various positions down the tube for these five patterns. In all cases, the driver section was 37" long and the dowel-filled section of pipe began at 10'0". Three curves are also drawn in each figure, but before we consider them, let us compare the different sets of points. The two sets

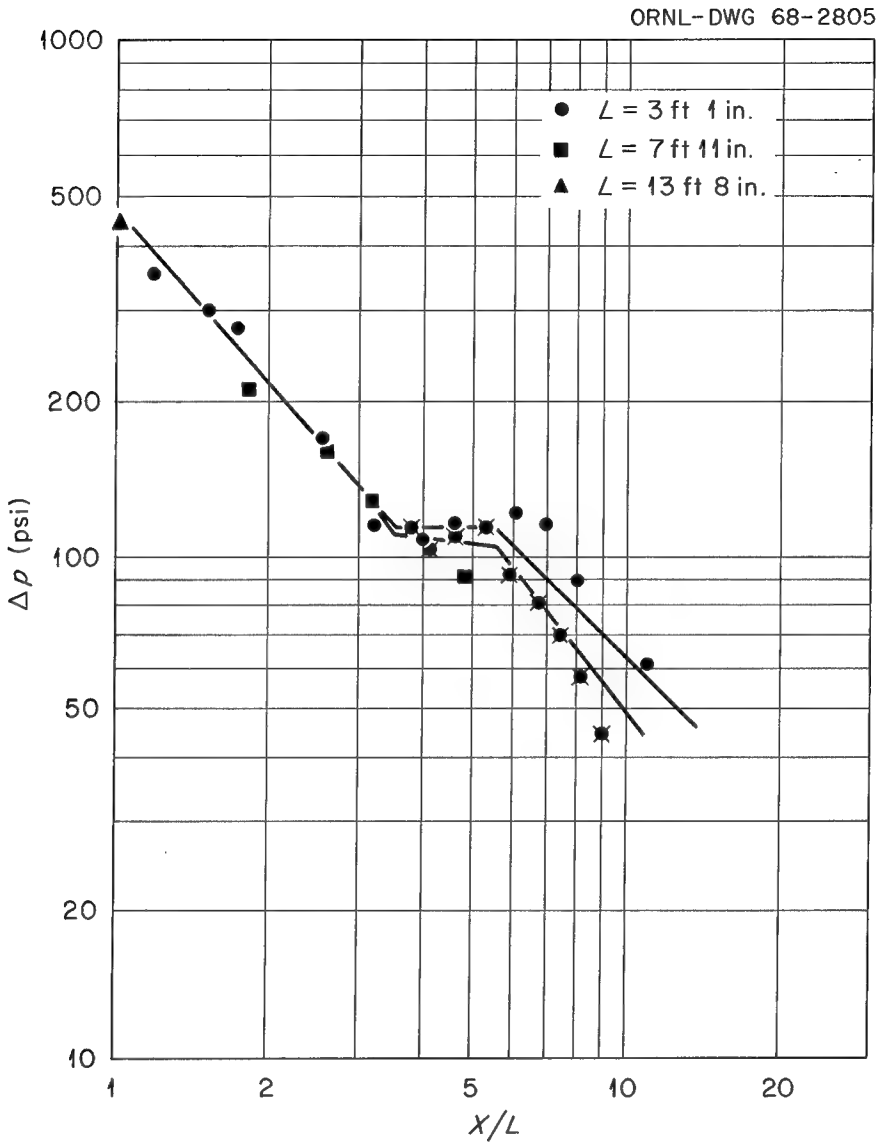

Figure 4. Peak overpressure in a tube with a threaded wall. Δp is the overpressure, X the distance down the tube, and L the length of the driver section. The points without wings are taken from Fig. 1 and refer to the bare tube. The points with wings refer to the tube with the threaded wall. The lower curve has been obtained by applying the correction factor of Eq. (3) to the upper curve.

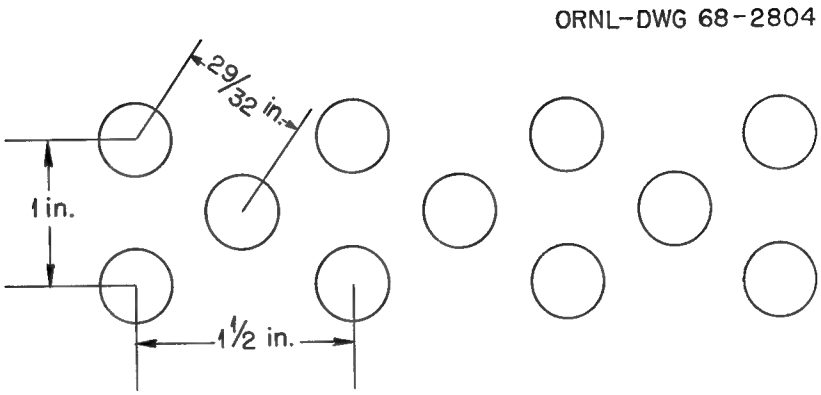

(a) FULL DENSITY

(b) TWO-THIRDS DENSITY

(c) TWO-THIRDS DENSITY

(d) ONE-THIRD DENSITY

(e) ONE-THIRD DENSITY

Figure 5. The arrangement of the holes in the base plate into which aluminum dowels could be screwed. The five patterns used are shown below, the crosses indicating filled holes.

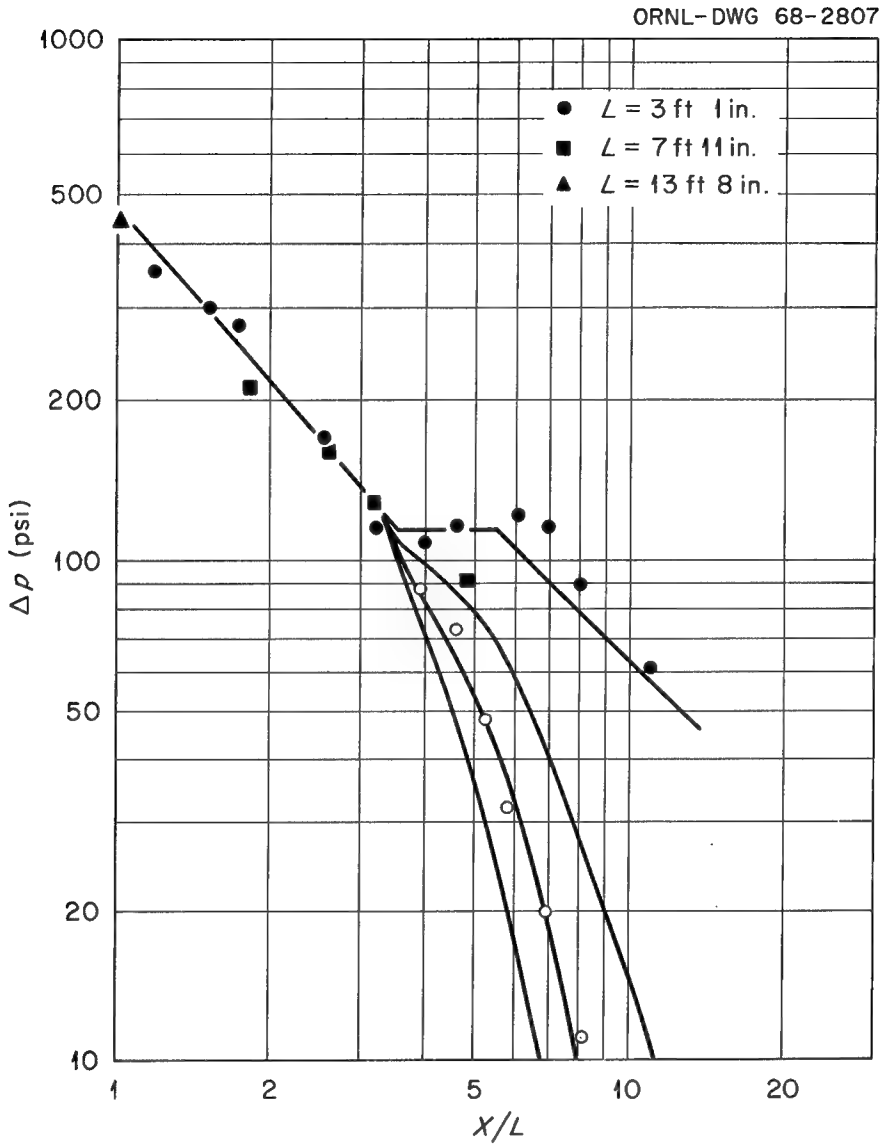

Figure 6a. Peak overpressure in a tube containing cylindrical obstacles. Δp is the overpressure, X the distance down the tube, and L the length of the driver section. The black points are taken from Fig. 1 and refer to the bare tube. The open points refer to positions inside the section of tube containing the cylindrical obstacles. The packing pattern is number (a) of Fig. 5. The lower curves have been obtained by applying the correction factor of Eq. (3) to the upper curve.

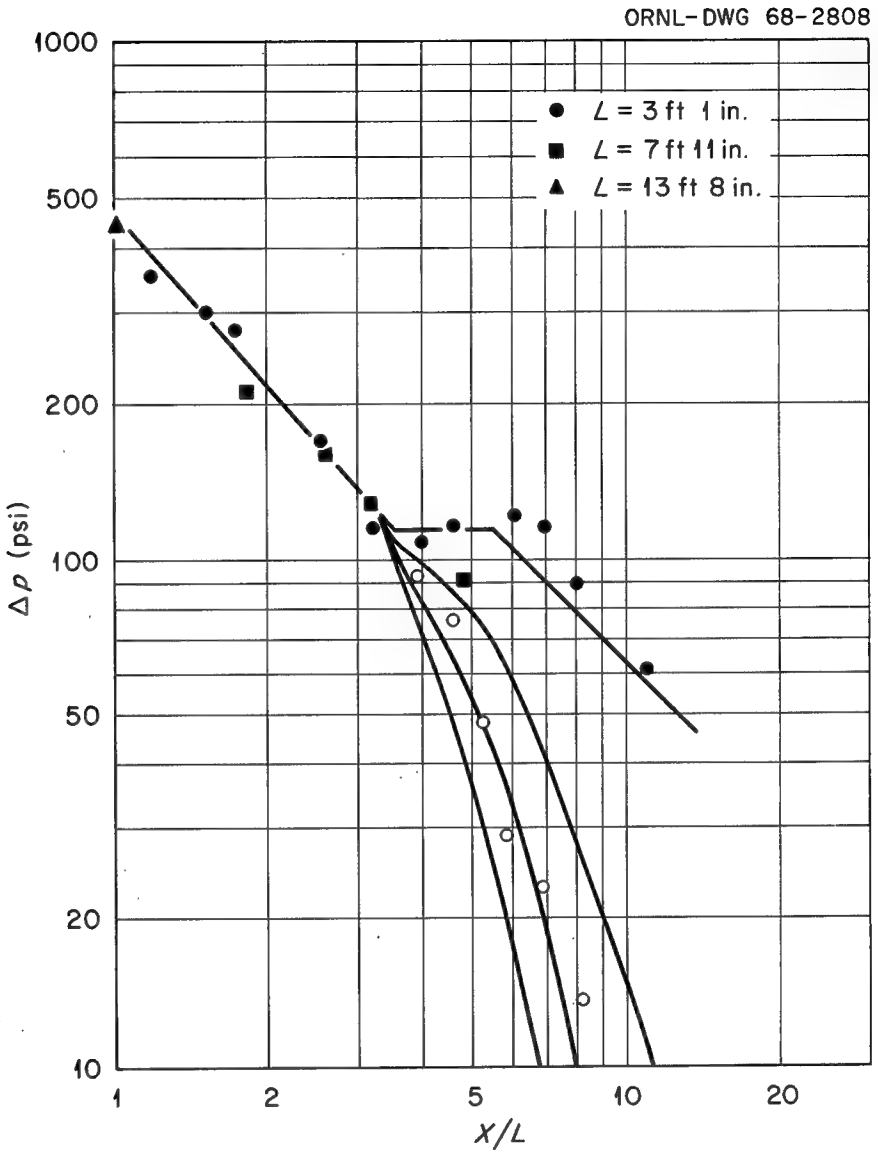

Figure 6b. Peak overpressure in a tube containing cylindrical obstacles. Δp is the overpressure, X the distance down the tube, and L the length of the driver section. The black points are taken from Fig. 1 and refer to the bare tube. The open points refer to positions inside the section of tube containing the cylindrical obstacles. The packing pattern is number (b) of Fig. 5. The lower curves have been obtained by applying the correction factor of Eq. (3) to the upper curve.

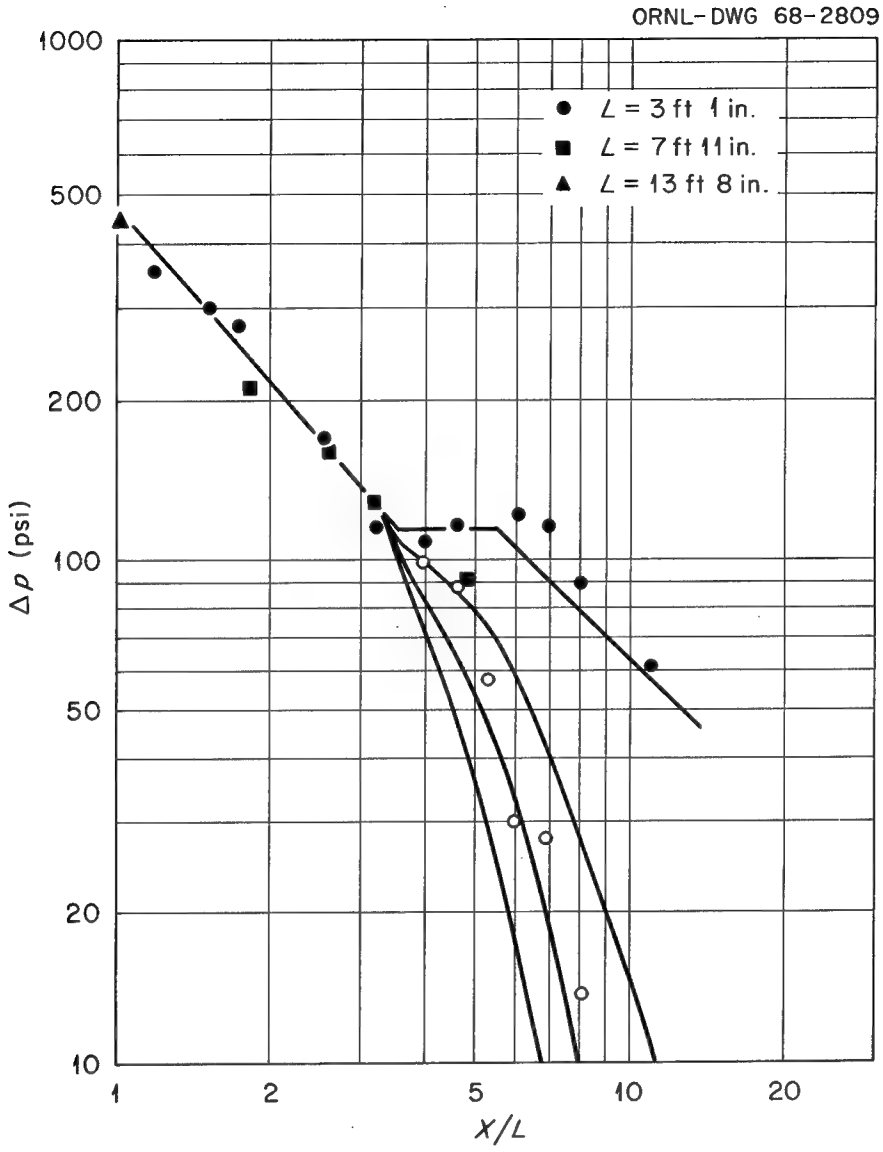

Figure 6c. Peak overpressure in a tube containing cylindrical obstacles. Δp is the overpressure, X the distance down the tube, and L the length of the driver section. The black points are taken from Fig. 1 and refer to the bare tube. The open points refer to positions inside the section of tube containing the cylindrical obstacles. The packing pattern is number (c) of Fig. 5. The lower curves have been obtained by applying the correction factor of Eq. (3) to the upper curve.

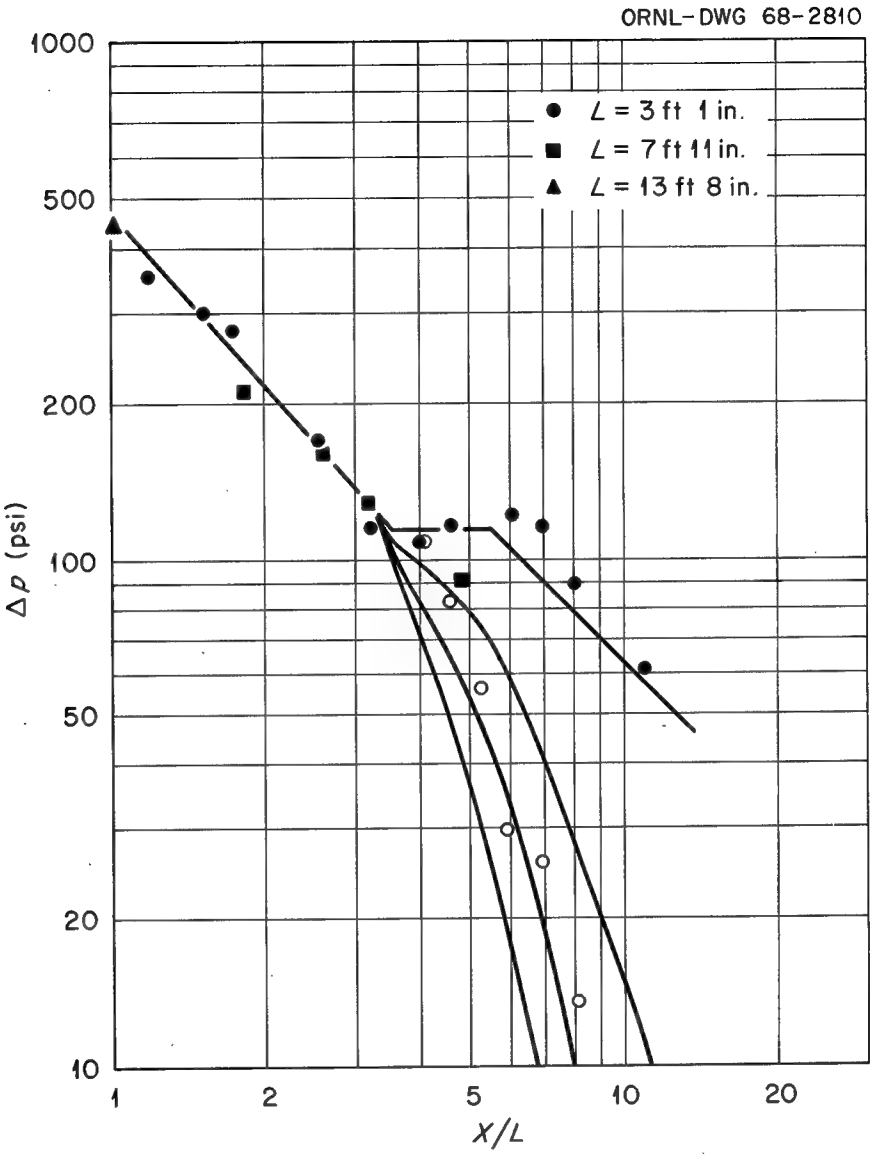

Figure. 6d. Peak overpressure in a tube containing cylindrical obstacles. Δp is the overpressure, X the distance down the tube, and L the length of the driver section. The black points are taken from Fig. 1 and refer to the bare tube. The open points refer to positions inside the section of tube containing the cylindrical obstacles. The packing pattern is number (d) of Fig. 5. The lower curves have been obtained by applying the correction factor of Eq. (3) to the upper curve.

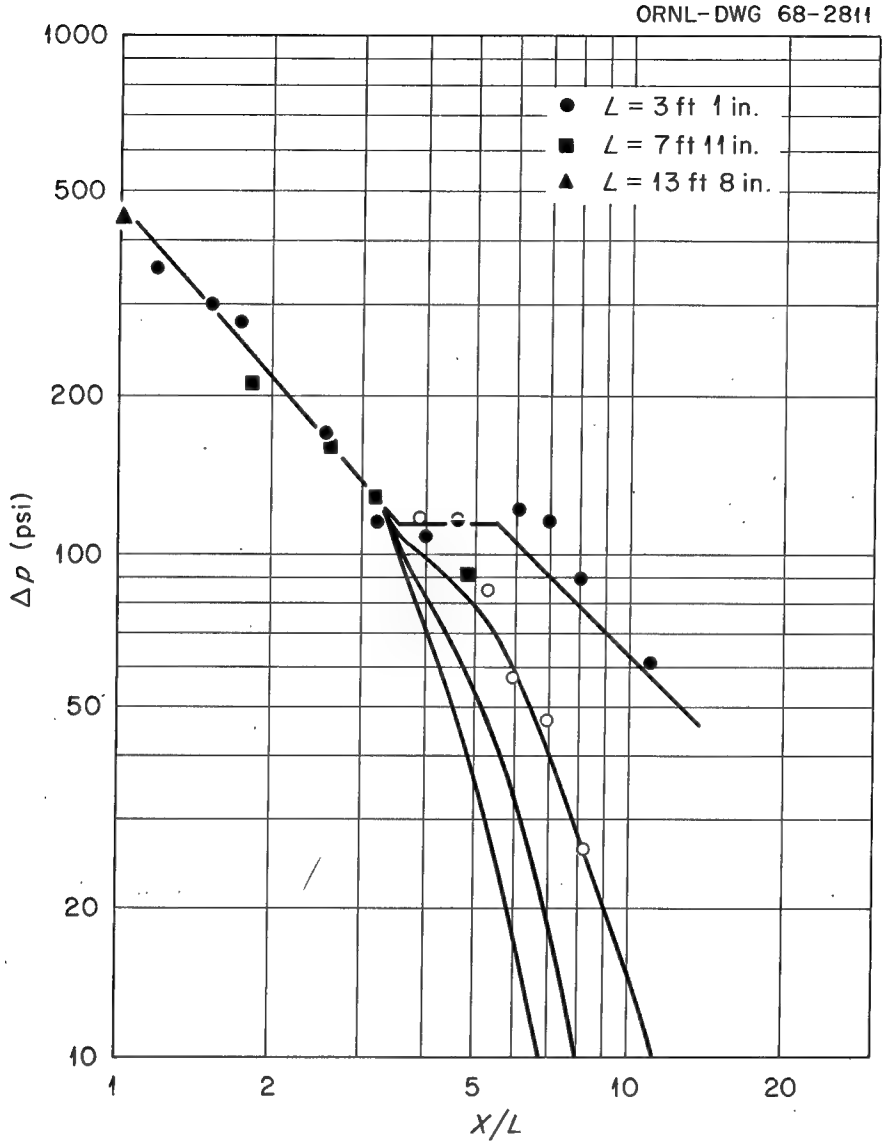

Figure. 6e. Peak overpressure in a tube containing cylindrical obstacles. Δp is the overpressure, X the distance down the tube, and L the length of the driver section. The black points are taken from Fig. 1 and refer to the bare tube. The open points refer to positions inside the section of tube containing the cylindrical obstacles. The packing pattern is number (e) of Fig. 5. The lower curves have been obtained by applying the correction factor of Eq. (3) to the upper curve.

of points corresponding to two-thirds density agree with one another fairly well, although there appear to be some differences in fine structure. The set of points corresponding to full density also agrees with these two, in contradiction to the expectation that it would equal the pressure in the bare tube corrected by a factor C, equal to the three-halves power of the factor $C_{2/3}$ that applies to two-thirds density. It appears that the local flow perturbations introduced by the dowels interfere with one another, and thus affect the value of the friction factor. Comparison of Figs. 6d and 6e, both referring to one-third density, shown further effects of such flow interference.

Not only does the friction factor vary with the pattern of dowel packing, but it may also vary with the Reynolds and Mach numbers of the flow. The Reynolds number of the flow behind a 100-psi shock moving into air at STP is about 7.7×10^5 when computed with the half-inch diameter of the aluminum dowels; the corresponding flow Mach number (flow velocity divided by ambient sound speed) is about 1.9. The corresponding numbers for a 10-psi shock are about 1.3×10^5 and 0.39, respectively. These overpressures roughly define the range covered in the experiments reported in Figs. 7. In this range, the skin friction coefficient c_f of isolated infinite cylinders lies between about 1.0 and 1.5.[9] Since the skin friction coefficient is referred to the projected area of the cylinders, rather than the wetted surface of the pipe, f is related to c_f by the equation

$$\frac{f}{c_f} = \frac{d\ h\ N}{\pi\ D} \qquad (4)$$

where d is the diameter of the cylinders, h is their height, N is the number of cylinders per unit length of pipe, and D is the diameter of the pipe. Finally, it is worth noting that the skin friction factor of cylinders may depend somewhat on the length-to-diameter ratio.

The three curves in Fig. 7 are based on values of f of 0.230, 0.153, and 0.0765. If we deduce a value of c_f from the best-fitting curve for each of the patterns (a) - (e), we find the values 0.76, 1.14, 1.14, 2.28, and 1.16, respectively. These values are roughly consistent with the range of values quoted above, but without more accurate values of the skin friction coefficient no better test of Eq. (3) is possible.

At this point it is worth digressing for a moment to consider again the square point at X/L = 4.8 in Fig. 1. As mentioned in Sec. 3, this point, which corresponds to a distance down the tube of 38', is probably low because of frictional resistance. If we use the nearby circular points, which correspond to distances down the tube of about 15', to find the pressure at X/L = 4.8 in the absence of friction, we find it to be about 115 psi. According to Eq. (3), the friction factor f of the bare tube is then about 0.007, which is not unreasonable for aged iron pipe.[5] (Actually, this value of f is only a crude estimate, since a slight change in the measured overpressure causes a much larger change in f.) A friction factor of 0.007 could mean that the rightmost circular points are slightly low. Thus their trend in the absence of friction might be nearly parallel to the line of slope -1 in Fig. 1, a possibility that must be borne in mind.

In their study of wall effects in shock tube flow, Emrich and Wheeler[10] also employed an exponential formula for the attenuation of

the overpressure. Their relaxation length, 420 diameters, corresponds to a friction factor of 0.008, in good agreement with what we have obtained above. It should be noted, however, that their value is an average of a large number of relaxation lengths measured in a variety of shock tubes, and that the individual values vary by as much as a factor of three from their average.

5. DISCUSSION

The discussion of the last section revolved around correlation of the experimental data by Eq. (3). However, even in the absence of a good correlation, the experimental data are extremely useful, representing scale models of the exposure of shelter tunnels to nuclear blast. The purpose of this section is to discuss the scaling by dimensional analysis of the problem of a shock wave normally incident on the open mouth of a cylindrical tunnel.

If its shape is given, the incident shock wave may be characterized by two parameters, which we choose here to be the shock overpressure Δp_{inc} and the energy per unit area of shock front E. The air into which the shock is moving has a density ρ_o and a pressure p_o. Since viscous effects are important, we ought to include the viscosity of the air in front of the shock or some other equivalent physical variable. For convenience, we combine the flow velocity behind the shock front (calculable from ρ_o, p_o, and Δp_{inc} via the Rankine-Hugoniot equations), the viscosity there (likewise calculable from the temperature

via the Rankine-Hugoniot equations), and the pipe diameter D, to obtain the Reynolds number of the flow behind the shock front; from this we obtain the corresponding Fanning friction factor f, which now replaces the viscosity. The pipe is determined by its diameter D and sufficiently many other lengths L_i necessary to specify uniquely the geometrical arrangement of its interior. Thus the overpressure Δp at any point ΔX down the pipe is a function of the variables Δp_{inc}, E, ρ_o, p_o, f, D, ΔX, and all the L_i. In dimensionless form

$$\frac{\Delta p}{\Delta p_{inc}} = F\left(\frac{E}{\Delta p_{inc} D}, \frac{\Delta p_{inc}}{p_o}, f, \frac{Li}{D}, \frac{\Delta X}{D}\right) \qquad (5)$$

Let us now consider the experiments performed with the orifice plates. Geometric similarity makes the last two dimensionless groups in Eq. (5) the same for the scale model as for the actual shelter tunnel. If we keep $\Delta p_{inc}/p_o$ the same, then the flow velocity behind incident shock front will be the same, and thus the Reynolds number of the flow will change owing to the change in diameter in going from the model to the full-scale tunnel. Fortunately, we are well into the range where the friction factor is independent of Reynolds number, and thus geometric similarity also guarantees equality of the friction factors for the model and the full-scale tunnel.

The tunnel-grid system described by Wigner in reference 1 consists of eight-foot concrete tunnels with a fiducial blast resistance between 100 and 200 psi. In all but one of the experiments reported in this paper, the incident overpressure was close to 125 psi, so that $\Delta p_{inc}/p_o$

was about the same for the model as for full scale. The total yields of the blasts to which such tunnels might be exposed probably lie in the range 0.1 to 10 megatons. The values of $E/\Delta p_{inc}D$ at the 125-psi radius for yields of 0.1, 1, and 10 megatons are 200, 440, and 940, respectively.[11] The value in the shock tube experiments using the 37" driver was 110, which is somewhat lower than the full-scale values but nearly of the right order of magnitude; for the 95" driver, $E/\Delta p_{inc}D$ was 160.

It is unlikely that the function F depends very strongly on the first two of its arguments, especially if they are large enough. Let us consider the first. $E/\Delta p_{inc}$ has the dimensions of length and gives the order of magnitude of the length of the incident blast wave. (If the blast wave is created by a surface burst of yield Y, then the distance R of the shock front from the explosion center when the shock overpressure is Δp_{inc} is $0.985\ E/\Delta p_{inc}$ when $\Delta p_{inc} \gg p_o$.[12] Here $E = Y/2\pi R^2$.) The length $3.33D/f$ on the other hand is the relaxation length of the overpressure due to interaction with the orifice plates. Hence, the quantity $(0.985E/\Delta p_{inc})/(3.33D/f) = 0.296 \cdot f \cdot E/\Delta p_{inc}D$ gives the ratio of the length of the incident blast wave to the relaxation length of the overpressure due to interaction with the orifice plates. If we pick a typical value of f of 0.15 for the 3-1/8" orifice plates, the values of this ratio for surface bursts with yields of 0.1, 1, and 10 megatons are 8.9, 19.5, and 41.7, respectively. Thus in the full-scale situations, the incident wave is long compared to the relaxation length of the overpressure due to interaction with the orifice plates.

This means that the incident wave would undergo only a small decrease in overpressure due to its longitudinal expansion in moving one relaxation length in the absence of the orifice plates. Increasing the length of the shock wave once it is long compared with the relaxation length should thus have no additional effect.

In the shock tube experiments with the 37" driver, $0.296 \cdot f \cdot E/\Delta p_{inc} D = 4.9$ when $f = 0.15$. However, here we know the length of the incident wave is approximately 10', and when $f = 0.15$, the relaxation length is about 7.4'. Thus the length of the incident wave is only 1.35 relaxation lengths instead of 4.9. The reason for the discrepancy is that the coefficient of 0.296 is based on the wave shape for the spherical blast wave from a point explosion, which of course is not right for the shock tube. (The actual wave shape is given in Fig. 10g of reference 2.) However, because of the "plateau" in the overpressure-distance curve in the shock tube, the overpressure of the incident wave would not decrease substantially in traversing the baffled section if the baffles were absent, which is exactly the situation desired. Hence, on this basis, we feel that small differences in the values of $E/\Delta p_{inc} D$ for the scale model and the full-scale case are unimportant. Furthermore, we are inclined to think that if $\Delta p_{inc} \gg p_o$, F does not depend much on the second argument in Eq. (5) for the reasons mentioned in connection with Eq. (1). Thus the attenuation should be relatively independent of the incident overpressure as long as the latter is large compared with the ambient pressure.

Our shock tube is a 1:24 scale model of an eight-foot shelter

tunnel. According to the results summarized in Fig. 3, for example, 320 feet of baffles with a 39% area blockage (corresponding to the 3-1/8" baffles) spaced 8 feet apart will reduce an incident overpressure of 125 psi to 10 psi. Furthermore, this spacing is nearly optimum; according to the data of Arredi, the friction factor for these baffles goes through a broad maximum near a spacing of one diameter, reaching a peak value of 0.22 at a spacing of about 3/4 D. If instead of a 39% area blockage, we use a 61% area blockage (corresponding to the 2-1/2" baffles) and keep the eight-foot spacing, 10 psi is reached in about 86 feet.

The threaded wall used in the second experiment had a relative roughness of 0.0271. In an eight-foot pipe with the same relative roughness, the height of the protuberances would be about 2.60". This is somewhat smaller than the protuberances in a tunnel blasted out of rock; moreover, the threads have a regularity to them that a rough rock wall does not. However, this regularity appears not to affect the friction factor, probably because of the close spacing of the threads: the friction factor corresponding to a sand-coated wall with a relative roughness of 0.027 is very close to 0.013. Furthermore, since the friction factor of a sand-coated wall varies as the 0.314 power of the relative roughness,[13] 10" protuberances in an eight-foot tunnel would produce a friction factor of only about 0.020. Hence, from the geometric point of view, the threaded wall is an adequate scale model of the interior of a tunnel blasted out of rock.

If the friction factor of the tunnel wall is 0.013, the ratio of

the length of the incident wave to the relaxation length due to wall drag is about 0.77, 1.7, and 3.5, respectively,for yields of 0.1, 1, and 10 megatons. In the model experiments, the length of the incident wave was about 10'; the relaxation length is about 85'. Hence, for this experiment, our scaling may not be right. Nevertheless, we feel fairly certain that the relaxation length for walls with relative roughnesses of the order of 0.1 are of the order of one to three hundred diameters.

A 24-fold magnification of one of the aluminum dowels yields a cylinder five feet long and a foot in diameter, which is approximately the size of a small human figure. The full-density pattern shown in Fig. 5 scales to a packing density of 5280 per linear mile in an eight-foot pipe, which is the density foreseen in Wigner's article. By examining the curves in Figs. 6a-e, we see that in the model experiments the friction factor f is always near 0.1, irrespective of which of the five patterns of packing is used. If f were the same in the full-scale case, then the ratio of the length of the incident wave to the relaxation length would be 5.9, 13.1, and 27.8 for yields of 0.1, 1, and 10 megatons, respectively. Actually in going from reduced to full scale, the Reynolds number of the flow increases by a factor of 24, but this would not change c_f enough to alter the conclusion that at full scale the incident wave is longer than the relaxation length. Hence, as with the orifice plates, the incident wave would not suffer much change in shock overpressure in traversing the baffled section if the baffles were absent, which is exactly the situation in the model experiments.

The experiments with the dowels indicate that the relaxation length is between about 20 and 40 diameters, the precise value depending on the density and pattern of packing. At full scale, this means that the relaxation length is in the neighborhood of 150 to 300 feet in an eight-foot tunnel. Hence, the occupants of the first few hundred feet of shelter tunnel will protect the rest, so that even if no baffles are provided, there is no chance of the shock waves sweeping for miles down occupied shelter tunnels. This point has been discussed earlier by Newman.[14]

REFERENCES

1. "Civil Defense," Publication No. 82 of the American Association for the Advancement of Science, Washington, D. C., 1966, H. Eyring (Ed.).

2. L. Dresner, "The Variation of Shock Overpressure with Distance in an Explosively Driven Shock Tube," ORNL-TM-1966, September 12, 1967.

3. B. Lewis and G. von Elbe, "Combustion, Flames, and Explosions of Gases," Academic Press, New York, 1961, p. 531.

4. J. von Neumann and R. D. Richtmyer, Journal of Applied Physics 21 232 (1950).

5. L. F. Moody, Trans. ASME 66 671 (144).

6. F. Arredi, Ricerche di Ingegneria, pp. 264-277, No. 6, Nov.-Dec., 1934-XIII.

7. H. Möbius, Physikalische Zeitschrift 41 202 (1940).

8. L. Schiller, Zeitschrift für angewandte Mathematik und Mechanik 3 2 (1923).

9. "A Survey of Reports on Experimental Studies of the Force Exerted on Model Structures by the Wind and by Blast Waves," J. E. Uppard, AWRE-E-6/67, May, 1967, Fig. 7; "The Drag on a Circular Cylinder in

a Shock Wave," V. C. Martin, K. F. Mead, and J. E. Uppard, AWRE-O-34/67, May, 1967.

10. R. J. Emrich and D. B. Wheeler, Jr., Physics of Fluids 1 14 (1958).

11. "The Effects of Nuclear Weapons,"Revised Edition, February, 1964 S. Glasstone (Ed.), U. S. Gov't. Printing Office, Wash., D. C., p. 134-5.

12. G. I. Taylor, Proc. Roy. Soc. A201 159 (1950).

13. H. Schlichting, "Grenzschicht-Theorie," G. Braun, Karlsruhe, 1951, p. 379.

14. "Attenuation of Shock Waves in Tunnel Shelters," John Newman, ORNL-TM-1622, September 8, 1966.

ORNL-4288
UC-38 — Engineering and Equipment

INTERNAL DISTRIBUTION

1. Biology Library
2-16. Civil Defense Project Library
17-19. Central Research Library
20-21. ORNL — Y-12 Technical Library Document Reference Section
22-41. Laboratory Records Department
42. Laboratory Records, ORNL R.C.
43. J. C. Bresee
44-53. C. V. Chester
54. H. C. Clairborne
55. N. E. Clapp, Jr.
56-65. L. Dresner
66. B. R. Fish
67. C. M. Haaland
68. R. L. Hahn
69. F. F. Haywood
70. G. J. Kidd
71. M. E. Lackey
72. C. E. Larson
73. J. L. Liverman
74. H. G. MacPherson
75-76. F. C. Maienschein
77. J. R. McWherter
78. J. P. Nichols
79. M. J. Skinner
80. L. E. Stanford
81. D. A. Sundberg
82. R. A. Uher
83. D. R. Vondy
84. J. L. Wantland
85. A. M. Weinberg
86. E. P. Wigner

EXTERNAL DISTRIBUTION

87. H. M. Agnew, Weapons Physics Division, Los Alamos Scientific Laboratory, Los Alamos, New Mexico
88. William Brown, Hudson Institute, Harmon-on-Hudson, New York
89. G. A. Coulter, Ballistic Research Labs, Aberdeen Proving Ground, Aberdeen, Maryland
90-100. L. J. Deal, Civil Effects Branch, Division of Biology and Medicine, U.S. Atomic Energy Commission, Washington, D.C.
101. Grace Kelleher, Institute for Defense Analyses, Arlington, Virginia
102. Jack Kelso, Defense Atomic Support Agency, Department of Defense, Washington, D.C.
103. N. E. Landdeck, Office of Civil Defense, Washington, D.C.
104. D. L. Lehto, U.S. Naval Ordnance Laboratory, White Oak, Silver Spring, Maryland
105. Billy McCormac, IITRI, 10 West 35th Street, Chicago, Illinois
106. Clarence Mehl, Sandia Corporation, Albuquerque, New Mexico
107. E. E. Minor, Ballistic Research Laboratory, Aberdeen, Maryland
108. D. L. Narver, Jr., Holmes and Narver, Inc., 828 S. Figueroa Street, Los Angeles, California
109. J. S. Newman, Department of Chemical Engineering, University of California, Berkeley, California
110. Edgar Parsons, Research Triangle Institute, Raleigh, North Carolina
111. L. Rudlin, U.S. Naval Ordnance Laboratory, White Oak, Silver Spring, Maryland
112. M. Rubenstein, Defense Atomic Support Agency, Department of Defense, Washington, D.C.
113. Col. Ralph Pennington, Advanced Research Projects Agency, Department of Defense, Washington, D.C.

114. Duane Sewell, Lawrence Radiation Laboratory, Livermore, California
115-124. W. E. Strope, Office of Civil Defense, Washington, D.C.
125. J. A. Swartout, Union Carbide Corporation, New York
126. William Taylor, Ballistic Research Laboratory, Aberdeen, Maryland
127. W. A. Whitaker, Air Force Weapons Laboratory, Kirtland Air Force Base, Albuquerque, New Mexico
128. William White, Stanford Research Institute, Stanford, California
129. Paul Zigmun, U.S. Naval Radiological Defense Laboratory, Hunter's Point, San Francisco, California
130. Laboratory and University Division, AEC, ORO
131-344. Given distribution as shown in TID-4500 under Engineering and Equipment category (25 copies — CFSTI)